iScience

CellPress
OPEN ACCESS

Article

Excess endocrine growth hormone in acromegaly promotes the aggressiveness and metastasis of triple-negative breast cancer

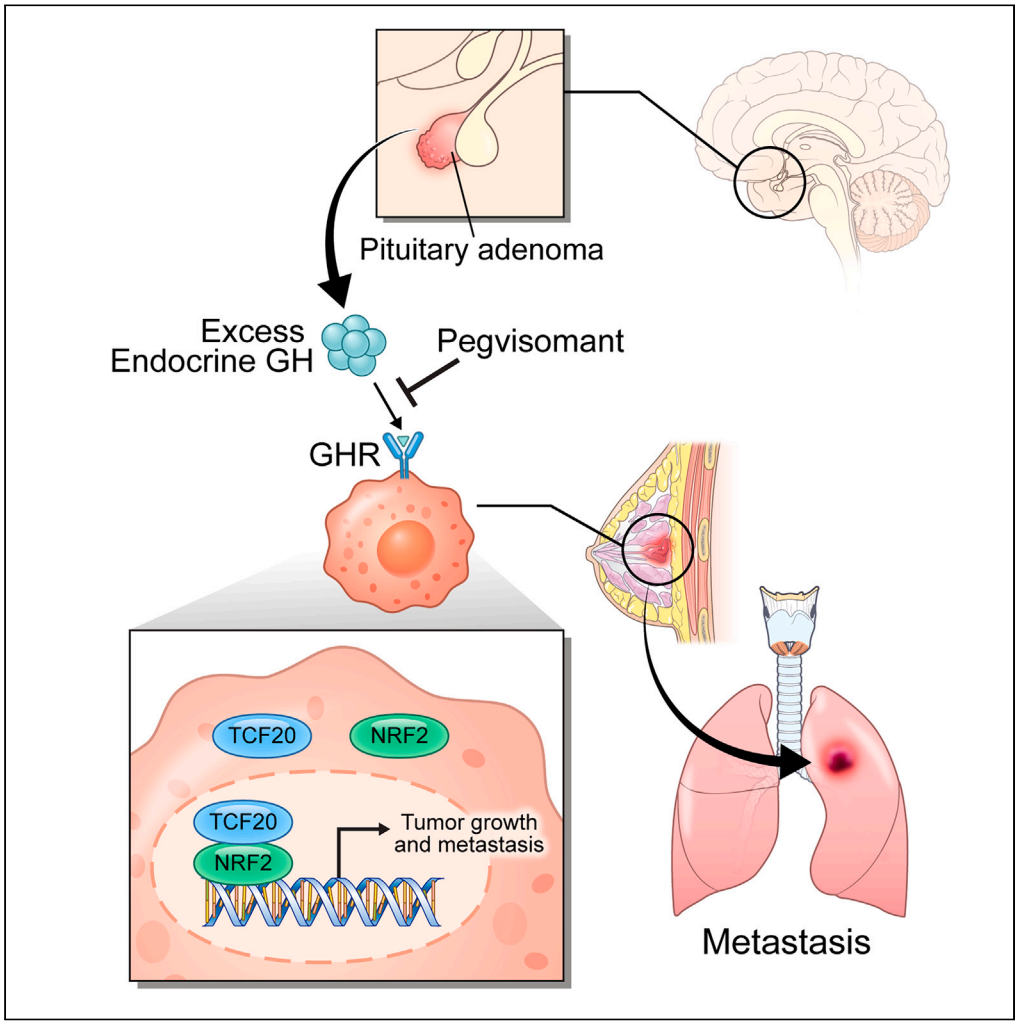

Chan Woo Kang, Ju Hun Oh, Eun Kyung Wang, ..., Young Seok Jo, Cheol Ryong Ku, Eun Jig Lee

cr079@yuhs.ac (C.R.K.)
ejlee423@yuhs.ac (E.J.L.)

Highlights

Excess endocrine GH promotes the growth and metastasis of TNBC cells

Excess endocrine GH activates NRF2 through TCF20-dependent pathway

Treatment of GHR antagonist inhibited TNBC metastasis in mouse with acromegaly

Kang et al., iScience 27, 110137
July 19, 2024
https://doi.org/10.1016/j.isci.2024.110137

iScience

CellPress
OPEN ACCESS

Article

Excess endocrine growth hormone in acromegaly promotes the aggressiveness and metastasis of triple-negative breast cancer

Chan Woo Kang,[1,5] Ju Hun Oh,[1,5] Eun Kyung Wang,[1] Yaru Bao,[1,2] Ye Bin Kim,[1,2] Min-Ho Lee,[3] Yang Jong Lee,[1] Young Seok Jo,[4] Cheol Ryong Ku,[1,*] and Eun Jig Lee[1,6,*]

SUMMARY

Pituitary adenoma-induced excess endocrine growth hormone (GH) secretion can lead to breast cancer development and metastasis. Herein, we used an acromegaly mouse model to investigate the role of excess endocrine GH on triple-negative breast cancer (TNBC) growth and metastasis. Additionally, we aimed to elucidate the molecular mechanism of transcription factor 20 (TCF20)/nuclear factor erythroid 2-related factor 2 (NRF2) signaling-mediated aggressiveness and metastasis of TNBC. Excess endocrine GH induced TCF20 activates the transcription of *NRF2* and NRF2-target genes to facilitate TNBC metastasis. Inhibition of GH receptor (GHR) and TCF20 activity using the GHR antagonist or small-interfering RNA-induced gene knockdown resulted in reduced tumor volume and metastasis, suggesting that excess endocrine GH stimulates TCF20/NRF2 pathways in TNBC and promotes metastasis to the lung. GHR inhibitors present an effective therapeutic strategy to prevent TNBC cell growth and metastasis. Our findings revealed functional and mechanistic roles of the GH-TCF20-NRF2 signaling axis in TBNC progression.

INTRODUCTION

Growth hormone (GH) is a peptide hormone that is mainly secreted by the somatotropic cells within the anterior pituitary gland in response to hypothalamic GH-releasing hormone (GHRH). GH is an anabolic hormone that induces growth in nearly every tissue and organ in the body and has the most distinct effect on cartilages and bones, especially during adolescence. GH is also responsible for the regulation of many basal metabolic functions; it is involved in carbohydrate and lipid metabolism and is a main regulator of hepatic insulin-like growth factor-1 (IGF-1) production.[1,2] The primary factors that regulate the secretion of GH in a pulsatile manner are GHRH, GH-inhibiting hormone, and somatostatin.[3] The dysregulation of GH secretion leads to GH excess or deficiency, either of which can cause several diseases.

Acromegaly is an insidious disease of exaggerated somatic growth and distorted proportion, arising from the hypersecretion of GH and IGF-1. Somatotroph adenomas, which are almost exclusively benign tumors of the anterior pituitary gland that secrete GH, are primarily responsible for acromegaly.[4,5] Pituitary gland tumors are the most common cause of head and neck tumors in adults after their 20s, accounting for 15% of all head and neck tumors. The exaggerated somatic growth and disfigurement caused by excess GH secretion is also associated with a wide range of systemic manifestations, such as excess bone and soft tissue growth, contributing to abnormal heights and exaggerated bone structures.[6]

Numerous clinical observations and experimental studies have consistently linked elevated levels of GH, as seen in conditions like acromegaly, to an increased risk of malignancy.[7–10] Notably, thyroid, colorectal, and breast cancers are the most commonly indicated as associated with acromegaly.[11–13] Conversely, patients with Laron syndrome, characterized by mutations in the GH receptor (*GHR*) gene, do not exhibit the cancer development.[14] Furthermore, breast cancer patient with high expression of GHR showed poor prognosis and survival compared to those with low GHR expression.[15] Insights from a meta-analysis involving 5 million women revealed a noteworthy association: a 10 cm increase in height corresponds to a 17% rise in the incidence of hormone-dependent breast cancer.[16,17]

GHR is expressed in the primary lesion of breast cancer, with notably elevated expression in metastatic hormone-negative breast cancer compared to hormone positive breast cancer.[15,18] The presence of autocrine human GH has been shown to facilitate the epithelial-to-mesenchymal transition (EMT), resulting in a metastatic phenotype[9] and increasing stemness.[19] While prior investigations have largely focused on experiments that involve the artificial induction of human GH overexpressed in cancer models,[7] our study takes a different approach, we

[1]Department of Internal Medicine Endocrinology, Institute of Endocrine Research, Yonsei University College of Medicine, Seoul, South Korea
[2]Brain Korea 21 PLUS Project for Medical Science, Yonsei University, College of Medicine, Seoul, South Korea
[3]University of Medicine and Health Sciences, New York, NY, USA
[4]Open NBI Convergence Technology Research Laboratory, Department of Internal Medicine, Yonsei University College of Medicine, Seoul, South Korea
[5]These authors contributed equally
[6]Lead contact
*Correspondence: cr079@yuhs.ac (C.R.K.), ejlee423@yuhs.ac (E.J.L.)
https://doi.org/10.1016/j.isci.2024.110137

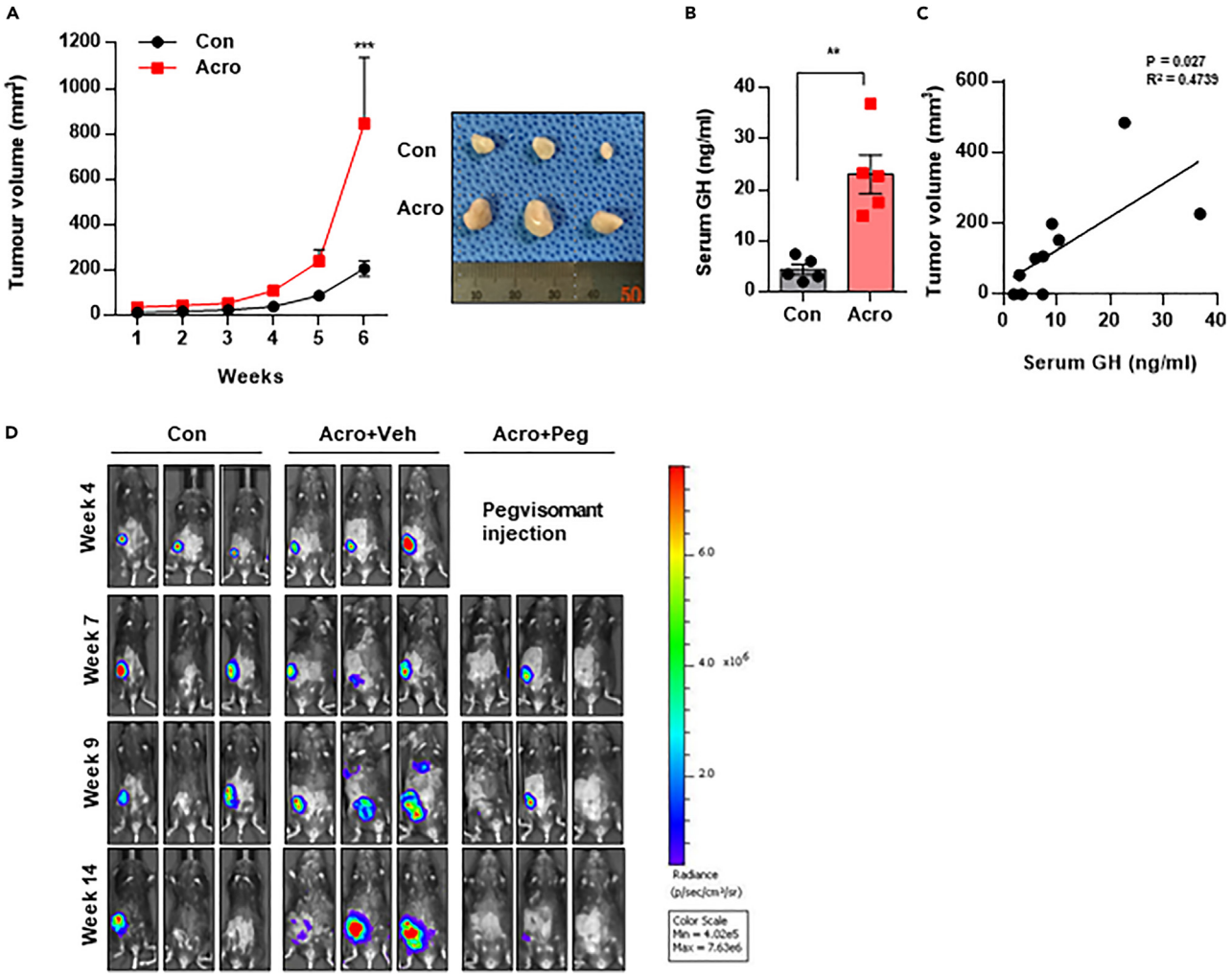

Figure 1. Excess endocrine GH increases primary tumor growth in mice with acromegaly

(A) Representative image and quantification of tumor volume.

(B) Serum GH concentration of Con and Acro mice.

(C) Positive correlation between serum GH and tumor volume.

(D) Con and Acro mice were mammary fat pad-inoculated with 2 × 10^6 Py230-Luc cells. Four weeks later, Acro mice were treated with pegvisomant (Peg) every day for 10 weeks. *In vivo* bioluminescence imaging of breast tumor after inoculation. All data are presented as the mean ± standard error of the mean. $^{**}p < 0.01$, $^{***}p < 0.001$ vs. Con mice.

employ an animal model characterized by the inherent endocrine elevation of GH, assessing variation in proliferation and metastasis following the implantation of identical cancer cells, providing a unique perspective. To the best of our knowledge, this study represents a pioneering investigation into cancer metastasis within the context of the acromegaly animal model. Additionally, our study differentiates itself by aiming to elucidate the mechanisms through which the excess endocrine GH, typical in acromegalic conditions, influences the tumor progression.

RESULTS

Excess endocrine growth hormone increases primary tumor growth in mice with acromegaly

To investigate the effect of excess endocrine GH on tumor growth, we used $Aip^{lox/lox}$ (Con mice) and rGHp-$Cre^{tg/+}$; $Aip^{lox/lox}$ mice (Acro mice), which were previously established to model the phenotype of human acromegaly.[12] Acro mice form pituitary adenomas that mimic human clinical features of acromegaly, including body size enlargement, elevated serum GH and IGF-1 levels, and impaired glucose tolerance and insulin resistance.[4–6,13,16] Notably, 50-week-old Acro mice exhibited mammary gland tumor development (Figure S1A). To generate an orthotopic breast cancer model in Acro and Con mice, we used a triple-negative breast cancer (TNBC) Py230 cell line, which is of the same strain. Py230 cells were orthotopically injected into the mammary gland of Con and Acro mice, and the tumor mass were measured. We observed an increase in the primary tumor size of Acro mice compared to Con mice six weeks after the injection of Py230 cells (Figures 1A and S1B). Serum GH levels were four-to 5-fold

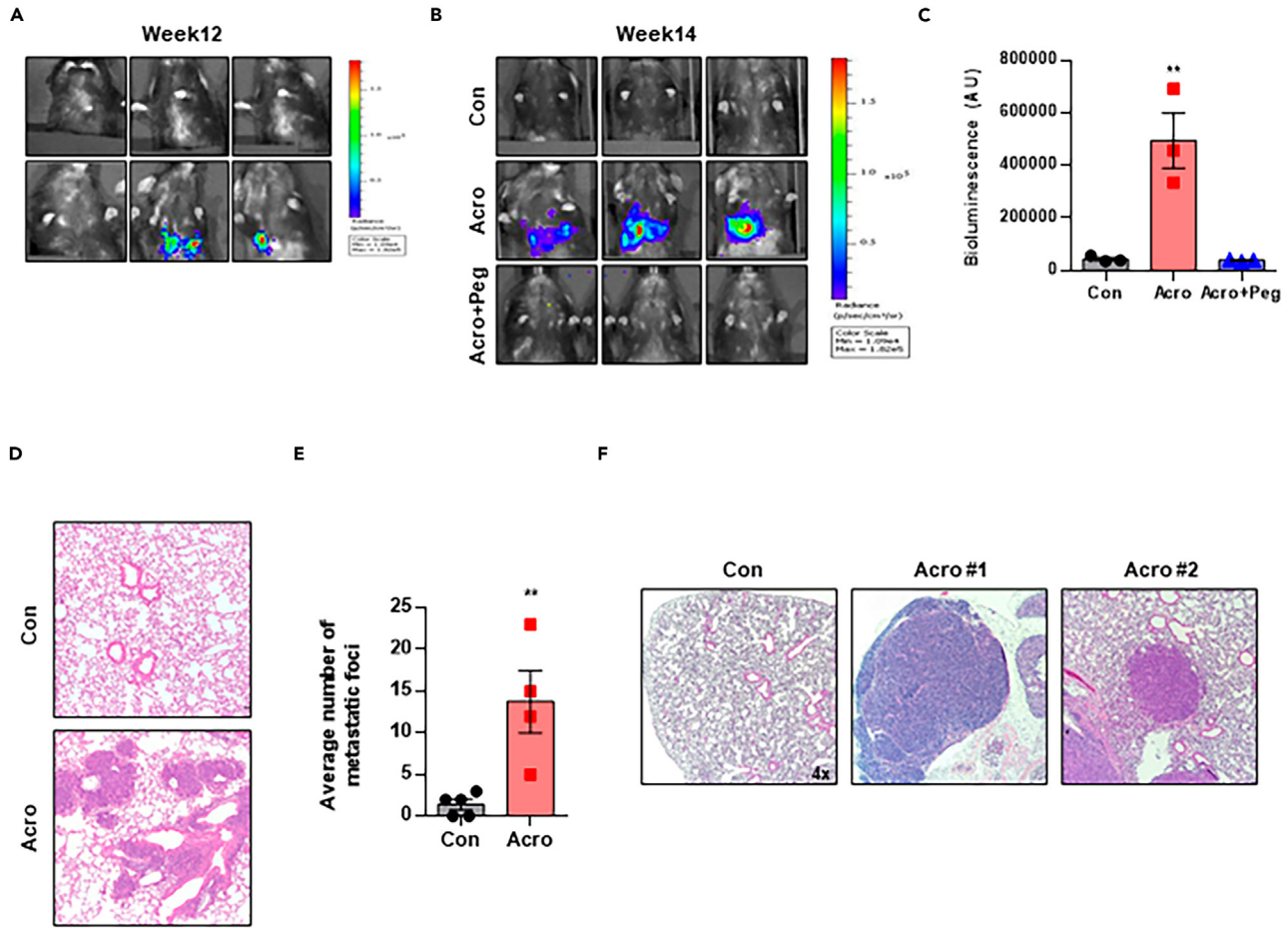

Figure 2. Excess endocrine GH signaling enhances metastasis

In vivo bioluminescence images of lung metastasis from mice at (A) 12 and (B) 14 weeks after inoculation with Py230-Luc cells (n = 4 mice per group).

(C) Quantification of lung metastasis bioluminescence intensity.

(D) Representative images of lung tissue sections stained with hematoxylin and eosin (H&E) 8 weeks after inoculation with Py230-Luc cells.

(E) Quantification of H&E-stained metastatic foci area of lung lesions.

(F) Representative images of lung tissue sections stained with H&E 16 weeks after inoculation with Py230-Luc cells. Images were obtained at 40× magnification. All data are presented as the mean ± standard error of the mean. $^{**}p < 0.01$ vs. Con mice.

higher in Acro mice than in Con mice. (Figure 1B). Of note, the tumor size and serum GH levels were positively correlated (Figure 1C). The concentrations of GH and IGF-1 in the mammary fat pad exhibited no discernible differences between Con mice and Acro mice (Figure S2). These data demonstrate that the disparity in tumor growth is attributed to excess endocrine GH rather than autocrine/paracrine GH.

Since excess endocrine GH promoted tumor growth, we next examined whether suppressed GH signaling was protective against tumor growth in Acro mice. The Py230 cells were engineered to stably express luciferase using lentiviral-mediated gene transfer (Py230-Luc cell) (Figure S1C). After the orthotopic injection of Py230-Luc cell, we confirmed tumor growth by assessing bioluminescence using IVIS (Figure 1D). The primary tumor size exceeded 100 mm^3 4 weeks after injection. Next, we subcutaneously administered pegvisomant, a GHR antagonist, around the peritumoral region to directly inhibit the GH signaling of Py230 cells. Pegvisomant-treated Acro mice exhibited decreased tumor size compared to vehicle-treated Acro mice. Notably, 10 weeks of pegvisomant treatment substantially reduced the tumor size. By contrast, vehicle-treated Acro mice exhibited increased tumors size approximately 1000 mm^3 (Figure 1D). These results clearly demonstrate the pivotal role of excess endocrine GH in facilitating the tumor growth.

Excess endocrine growth hormone signaling enhances tumor invasion

TNBC is a highly invasive disease that often metastasizes to the lung. As shown in Figure 1D, at week 9, compared with Con mice, vehicle-treated Acro mice exhibited increased bioluminescence in the lung. To identify the role of excess endocrine GH in tumor invasion and metastasis, we further investigated the metastatic tumors in the new Acro mice group. Compared to the Con mice, the Acro mice showed increased bioluminescence in the lung after 12 weeks (Figure 2A). After 14 weeks, we had to euthanize the Acro mice group owing to breathing

difficulties in the animals caused by serious lung metastatic burden. By contrast, bioluminescence was hardly detected in the lungs of Con and pegvisomant-treated Acro mice (Figures 2B and 2C). Consistent with the bioluminsescence distribution results, hematoxylin and eosin (H&E) staining showed that lung colonization was largely elevated in Acro mice compared with Con mice 8 weeks after Py230 cell injection (Figures 2D and 2E). Acro mice exhibited a significantly higher number of lung metastatic foci compared with Con mice (Figures 2D and 2E). 16 weeks after Py230 cell injection, lung metastatic burden and tumor growth significantly increased in Acro mice (Figures 2F and S3A). We further measured bioluminescence in other organs where breast cancer metastasizes, such as the liver, brain, bone, and lymph nodes. No bioluminescence was observed in organs other than the lung (data not shown). In addition, both Con mice and Acro mice had no liver metastasis (Figures S3B and S3C). These results suggest that TNBC exposed to excess endocrine GH is more prone to the metastasis.

Exogenous growth hormone induces breast tumor growth and invasion in triple-negative breast cancer cells

We investigate the effect of recombinant human GH (rhGH) on the TNBC cell line. We confirm that the expression of growth hormone receptors (GHRs) in TNBC cells, including MDA-MB-231, Hs578T, Py230, and HCC1806 (Figure 3A). Notably, the phosphorylation of signal transducer and activator of transcription (STAT)5, a key component of GH signaling, significantly increased under exogenous rhGH treatment in all TNBC cell lines examined (Figure 3A). To examine whether the effects of rhGH on tumor growth *in vivo* are reproduced *in vitro*, proliferation assays were performed. rhGH accelerated cell proliferation in MDA-MB-231, HCC1806, Hs578T, and Py230 cells, mirroring the results observed in *in vivo* tumor growth in Acro mice (Figure 3B). Furthermore, we examined the role of GH on cell migration and invasion in TNBC cells. Exogenous rhGH treatment enhanced cell invasion compared to PBS-treated TNBC cells (Figure 3C). Moreover, a dose-dependent acceleration of cell migration was observed in the Py230 and HCC1806 cell lines with rhGH treatment (Figures 3D and 3E). Considering the expression of GHR TNBC cell lines, we investigated whether inhibiting its expression would affect TNBC cell growth. We employed siRNAs to knock down *GHR* expression in Py230 cells, and confirmed the efficacy of siGHR in Py230 cells (Figure S4A). The colony formation in Py230 cells treated with siGHR was significantly decreased than that of siCON-treated Py230 cells (Figure 3F). These findings indicate that exogenous GH enhances TNBC cell growth, migration, and invasion.

Excess endocrine growth hormone activates nuclear factor erythroid 2-related factor 2 through the growth hormone receptor/transcription factor 20-dependent pathway

To investigate the molecular mechanism underlying excess endocrine GH in TNBC cellmetastasis, we utilized a mouse tumor metastasis RT^2 profiler PCR array (RT^2 array) to analyze both the primary tumor and lung metastatic lesions. As expected, the primary tumor and metastatic lesions in Acro mice exhibited the upregulation of several metastasis-associated genes. Consistent with previous studies,[20] GH induced alterations in the levels of EMT-related mediators, including the upregulation of *Src*,[21] *Myc*,[22] *MMP2*,[9] *FN1*,[23] and *CDH6*[24] and the downregulation of *PTEN*[25] in both primary tumor and lung metastatic lesions of Acro mice (Figure 4A). Interestingly, we found a significant upregulation of the TCF20 gene in both primary tumor and lung metastatic lesion, but its association with GH signaling has not been yet reported. This led us to hypothesize that TCF20 may be regulated by the excess endocrine GH, and thus, plays a role in TNBC metastasis.

TCF20, a 220 kDa multidomain nuclear protein present in various cells and tissues, serves as a transcriptional coactivator of NRF2, regulating the expression of the autophagy receptor p62.[26] Although NRF2, the master regulator of the cellular antioxidant program, can have detrimental effects when persistently activated,[27–29] whether the activation of the TCF20/NRF2 axis promotes TNBC metastasis remains unclear. To address this, we examined the impact of excess endocrine GH-induced TCF20/NRF2 activation in TNBC metastasis in acromegaly mice. Consistent with RT^2 array results, *TCF20* was upregulated in both primary and lung metastatic lesions, as observed by Real-time PCR analysis (Figure 4B). To further confirm the relationship between excess GH and TCF20 activation, we examined the mRNA expression of *TCF20*, *NRF2*, and NRF2-target genes in TNBC cell lines. The expression of *TCF20,* and antioxidant genes including *NRF2*, *NQ O -1*, and *Ho-1* were upregulated in Hs578T, Py230, and HCC1806 cells treated with exogeneous rhGH (Figure 4C). The protein level of TCF20 was induced by rhGH in a dose dependent manner (Figure 4D). To examine the nuclear translocation of GH-induced NRF2, we separated the cytoplasmic and nucleur protein fractions. Notably, rhGH treatment increased NRF2 expression in the nuclear fraction of Py230 and HCC1806 cells (Figures 4E and 4F). Additionally, the protein level of HO-1, the target gene of NRF2, was elevated in the cytoplasmic fraction upon rhGH treatment in Py230 and HCC1806 (Figures 4E and 4F). These findings strongly suggest a robust association between TCF20/NRF2 signaling and GH-induced TNBC cell growth and metastasis.

Growth hormone receptor and transcription factor 20 inhibition attenuate growth hormone-induced triple-negative breast cancer metastasis

Given the observed increase in TCF20/NRF2 and antioxidant gene expression after exogenous GH treatment in TNBC cells, we postulated that the GHR/TCF20/NRF2 axis is implicated in TBNC metastasis. To verify this hypothesis, we used siRNAs to knockdown *GHR* and *TCF20* expressions in TNBC cells (Figure S4). Consistent with previous results, exogenous rhGH treatment increased *TCF20*, *NRF2*, and antioxidant gene (*Nqo-1* and *Ho-1*) expressions in the siCON group (Figure 5A–C). In contrast, knocking down *GHR* or *TCF20* using siRNA abolished the upregulation of TCF20/NRF2 and expression of *Nqo-1* and *Ho-1* (Figures 5A–5C). In line with the Real-time PCR results, treatment with rhGH induced significant nucleus translocation of STAT5 and NRF2, along with increase in the cytosolic protein expression of HO-1 in the siCON group. In contrast, the effect of GH on NRF2 translocation and HO-1 expression decreased in siGHR- and siTCF20-treated TNBC cells (Figures 5D and 5E). To further investigate the effects of inhibiting the GHR/TCF20/NRF2 signaling axis on the metastatic characteristics of TNBC, we knocked down *GHR* or *TCF20* in HCC1806 and Py230 cells. The result showed reduced invasion and migration compared to

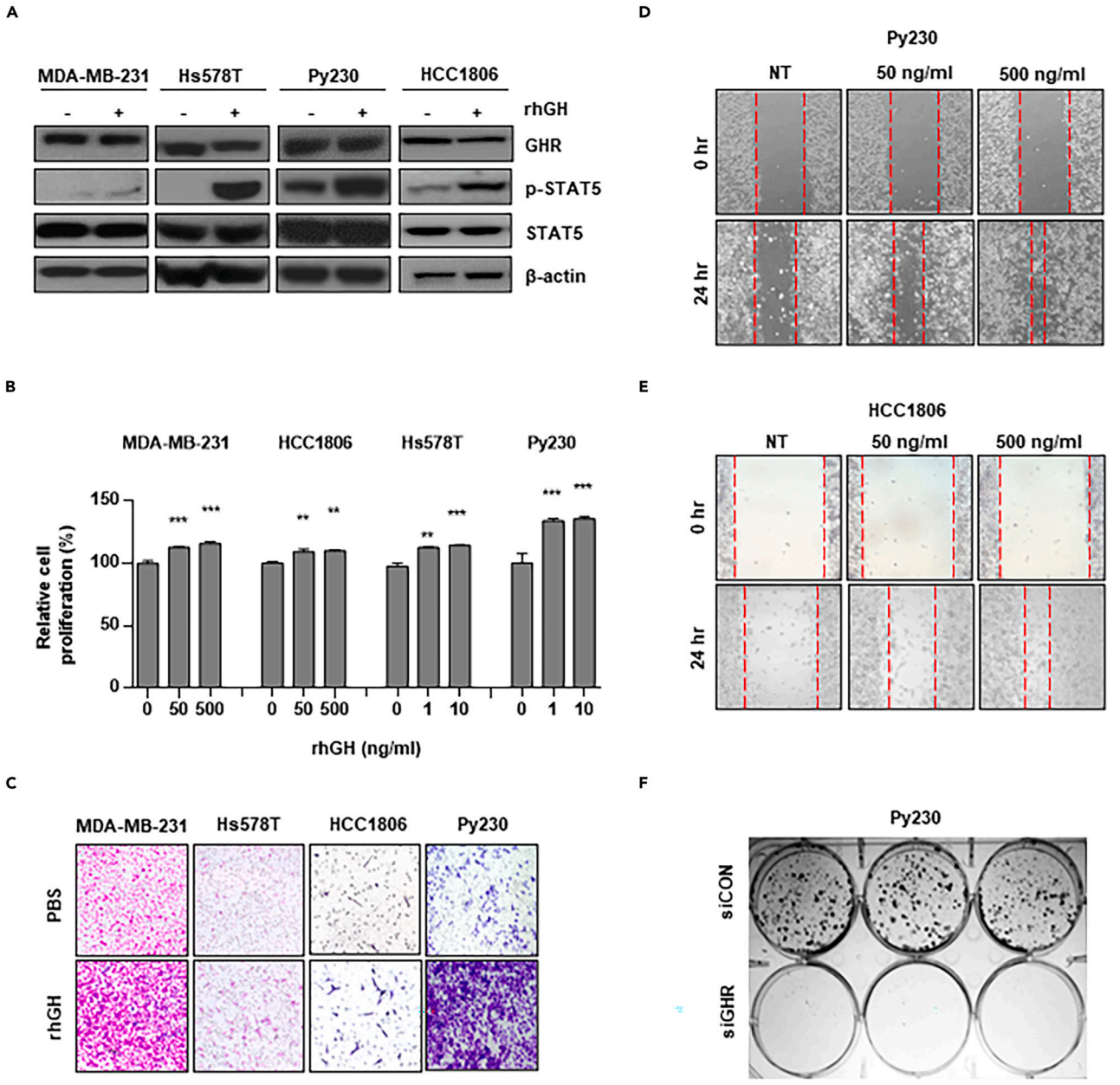

Figure 3. Exogenous GH induces growth and invasion in TNBC cell lines

(A) Effects of GH on the phosphorylation levels of signal transducer and activator of transcription 5, which indicates GH reaction, in MDA-MB-231, Hs578T, Py230, and HCC1806 cells. Each cell line was treated with recombinant human GH (rhGH) (500 ng/mL). The expression levels of indicated proteins were detected by western blot analysis using the indicated antibodies.

(B) The (3-(4, 5-dimethylthiazolyl-2)-2, 5-diphenyltetrazolium bromide) assays were performed to determine cell proliferation following treatment with the indicated dose of rhGH for 48 h (n = 4, biological replicates) in MDM-MB-231, HCC1806, Hs578T, and Py230 cells.

(C) Representative images of invasion assay in MDA-MB 231, Hs578T, HCC1806, and Py230 cells treated with phosphate-buffered saline or rhGH (500 ng/mL) for 24 h. Wound healing assay was performed to determine cell migration.

The migrated (D) Py230 and (E) HCC1806 cells (n = 4, biological replicates) were visualized using a microscope. rhGH was treated with indicated doses for 24 h.

(F) Colony formation assay of Py230 cells transfected with siCON or siGHR. Cells were grown in the absence or presence of rhGH (500 ng/mL) for 14 days. All cells were fixed and stained with crystal violet. All data are presented as the mean ± standard error of the mean. $^{**}p < 0.01$, $^{***}p < 0.001$ vs. non-treated control.

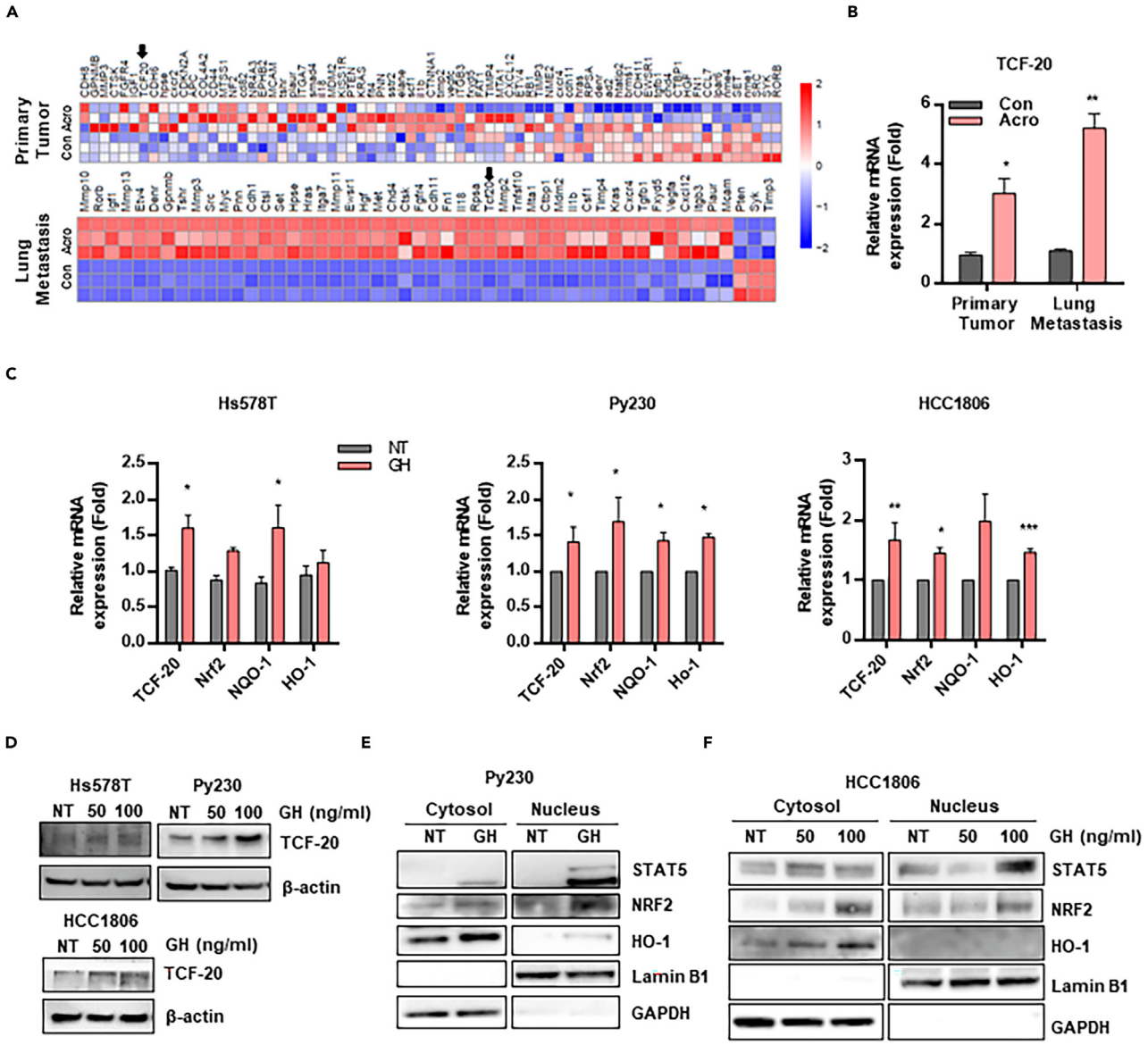

Figure 4. Excess endocrine GH activates nuclear factor erythroid 2–related factor 2 (NRF2) through the GH receptor/transcription factor 20 (TCF20)-dependent pathway

(A) RT^2 array demonstrating the differential expression of genes between the Con and Acro mice primary tumor or lung metastatic lesion.

(B) Real-time PCR analysis of *TCF20* mRNA expression in Con and Acro mice confirmed the transcriptomics data shown in (A).

(C) Real-time PCR analyses of *TCF20*- and *Nrf2*-target genes in Hs578T, Py230, and HCC1806 cells (n = 4). Results represent the mean of at least three independent experiments. *$p < 0.05$, **$p < 0.01$ vs. non-treated control.

(D) Western blot analysis showing the dose-dependent effect of recombinant human GH (rhGH) on the expression of TCF20 in Hs578T, Py230, and HCC1806 cells. Each cell line was treated with the indicated doses of rhGH for 24 h.

(E and F) Western blot analysis of the indicated cytosol and nucleus proteins (E) Py230 and (F) HCC1806 cells treated with the indicated doses of rhGH for 24 h.

rhGH-treated siCON HCC1806 and Py230 cells (Figures 5F–5I). Taken together, these results suggest that GH-induced TCF20 activation can promote TNBC cell metastasis by upregulating *NRF2* and NRF2 target genes.

Excess endocrine growth hormone induces transcription factor 20 and antioxidant proteins in the metastatic lesion of acromegaly mice

To validate the upregulation of TCF20 in excess endocrine GH-induced lung metastasis, we conducted immunohistochemistry on the lung tissues of the Con, Acro, and pegvisomant-treated Acro orthotopic breast cancer model. As shown in Figure 6A, TCF20 protein expression

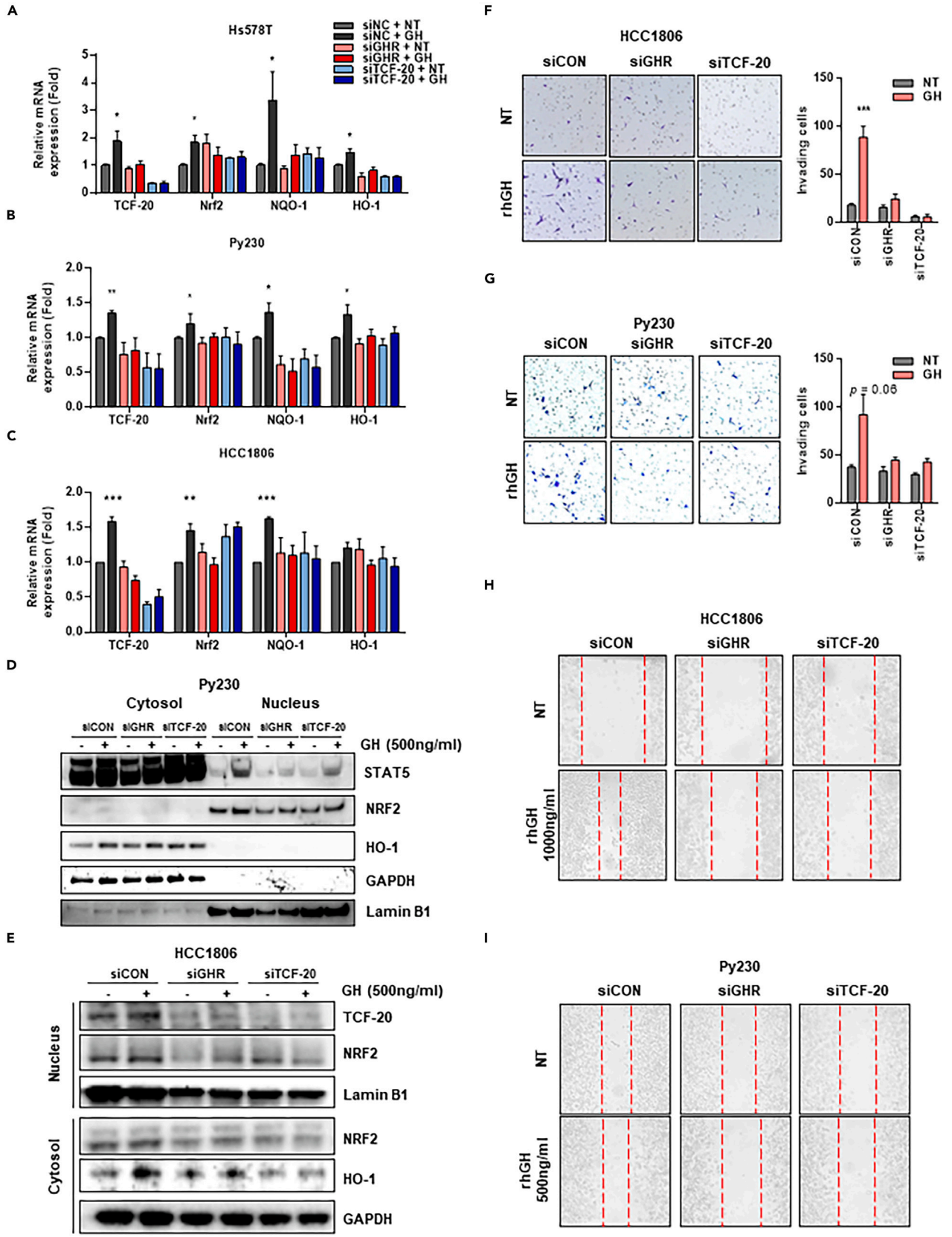
A
Hs578T
siNC + NT
siNC + GH
siGHR + NT
siGHR + GH
siTCF-20 + NT
siTCF-20 + GH
Relative mRNA expression (Fold)
TCF-20
Nrf2
NQO-1
HO-1
B
Py230
C
HCC1806
D
Py230
Cytosol
Nucleus
siCON
siGHR
siTCF-20
GH (500ng/ml)
STAT5
NRF2
HO-1
GAPDH
Lamin B1
E
HCC1806
Nucleus
Cytosol
F
HCC1806
NT
rhGH
Invading cells
G
Py230
p = 0.06
H
HCC1806
rhGH 1000ng/ml
I
Py230
rhGH 500ng/ml

Figure 5. GHR and TCF20 inhibition attenuates GH-induced TNBC metastasis

(A–C) Real-time PCR analyses of *TCF20*- and *Nrf2*-target genes in (A) Hs578T, (B) Py230, and (C) HCC1806 cells ($n = 3$). Results represent the mean of at least three independent experiments. *$p < 0.05$, **$p < 0.01$, ***$p < 0.001$ vs. siCON-transfected and non-treated (NT) control.

(D and E) Western blot analysis of the indicated cytosol and nucleus proteins of small interfering ribonucleic acid-transfected (D) Py23Ind (E) HCC1806 cells treated with the indicated dose of recombinant human GH (rhGH) for 24 h. (F, G) *GHR* or *TCF20* knockdown in (F) HCC1806 and (G) Py230 cells decreased tumor cell invasion through the Matrigel-coated transwell membranes ($n = 4$ biological replicates). Invading cells were quantified and indicated in the bar graph.

(H and I) Wound healing assay was used to determine cell migration in (H) HCC1806 and (I) Py230 cells. rhGH was treated with indicated doses for 36 h. All data are presented as the mean ± standard error of the mean. *$p < 0.05$, **$p < 0.01$, ***$p < 0.001$ vs. siCON-transfected and NT control.

was significantly increased in the lung colonization region along with GHR expression. Conversely, TCF20 expression was abolished in Acro mice treated with pegvisomant (Figures 6A and S5). We next examined the expressions of NRF2, HO-1, and NQO-1 in these lung tissues to validate the significance of the TCF20/NRF2 signaling axis in excess endocrine GH-induced tumor metastasis. Consistent with Figure 6A, NRF2, NQO-1, and HO-1 were notably enriched in the lung colonization region (Figures 6B and S5), providing confirmation that excess endocrine GH contributes to the enhanced growth and metastasis of TNBC through the activation of the TCF20/NRF2 signaling pathway.

DISCUSSION

In this study, we demonstrated that excess endocrine GH promotes tumor development and metastasis in acromegaly mouse models by boosting antioxidant genes. Excess endocrine GH acts as an antioxidant by activating TCF20 and NRF2, reducing oxidative stress and enhancing TNBC aggressiveness and metastasis. These results align with previous findings indicating that antioxidants, can stimulate tumor development and metastasis.[27,29]

Non-pituitary growth hormone (npGH) expression is well established in extrapituitary tissues, and previous studies have demonstrated the pro-tumorigenic impact of npGH on the tumor microenvironment.[23,30–33] In this study, we aimed to investigate the influence of excess endocrine GH on TNBC progression. Consequently, we investigated whether the effects of npGH in the tumor microenvironment could be linked to tumor growth in an Acro model. Upon measuring npGH and IGF-1 levels in the mammary fat pads of Con and Acro mice, no significant differences were observed (Figure S2). This result suggests that the increased tumor growth in the Acro model is likely attributed to the effects of excess endocrine GH. Although pituitary-secreted GH and npGH exhibit structural homogeneity, further research is needed to elucidate the specific physiological role between pituitary-secreted GH and npGH.

Pegvisomant is known as the treatment for acromegaly, and its anti-tumor effect has been demonstrated in various xenograft models for different types of tumors.[34] However, there are no reports on the anti-tumor effect of a GHR antagonist in an acromegaly animal model. In this study, we provide the evidence that excess endocrine GH in acromegaly promotes tumor growth and metastasis, and that GHR antagonist can inhibit tumorigenicity in the acromegaly animal model (Figures 1 and 2). In order to preclude the influence of circulating IGF-1, we administered pegvisomant specifically around the primary tumor site rather than systemically. Our results suggest that the decreased tumor growth observed in Acro mice treated with pegvisomant is the direct effect of GH. (Figure 1D). We further confirmed that IGF-1 treatment had any effect on the TCF20/NRF2 axis in TNBC cells (Figure S6). These results indicate that excess GH is sufficient for tumor growth and metastasis.

Previous studies established immunocomprised xenograft mouse model for tumor metastasis. However, this model lacks consideration for factors like the primary tumor's origin, tumor microenvironment, and immune responses – crucial elements for a comprehensive understanding of typical tumor metastasis processes.[25,34] In contrast, we established an orthotopic model for tumor metastasis using immunocompetent mice. This model allows us to investigate the role of excess GH on key metastasis steps, including primary tumor growth, detachment, intravasation, immune evasion, survival in circulation, extravasation, and colonization in a distant organ.

Previous studies have established that sex steroids, including estrogen, have the ability to regulate cell sensitivity to GH through multiple mechanisms.[35] Particularly, estrogens can induce the expression of SOCS-2 and SOCS-3, which subsequently negatively regulate the GHR-JAK2-STAT5 signaling pathway, resulting in a reduction in transcriptional activity in liver.[36] To investigate the potential impact of differences in estrogen levels on GH action, we examined estrogen concentrations. The serum estrogen levels in Con and Acro mice were found to be comparable (Con 155 ± 8.3 vs. Acro 147.8 ± 13.4 pg/mL) (Figure S7). Additionally, there was no difference in fertility between Con and Acro mice. Therefore, it can be assumed that GH acts as a major effector in tumor progression, at least in this context.

In vitro experiments were conducted using TNBC cell lines to validate the proliferative and metastatic effects of exogenous GH. To assess colonization, a pivotal stage in tumor development and metastasis, a colony formation assay was employed. Inhibition of GH signaling demonstrated a notable decrease in colony formation (Figure 3F). Conversely, treatment with exogenous GH significantly heightened cell invasion and migration in the tumor cells compared to the control cells (Figures 3 and 5). These results reinforce the contribution of GH to TNBC metastasis, aligning with the observations in the Acro mice study.

Antioxidants, such as NRF2 and its target genes, have been demonstrated to accelerate cancer progression and metastasis.[27,29] Antioxidants protect primary tumor cells from reactive oxygen species (ROS) and DNA damage.[28,37] GH reduces oxidative stress and prevents cell senescence.[16,30,38] Excess endocrine GH induces the expression of *TCF20*- and *NRF2*-target genes. Our findings from orthotopic breast cancerstudy in Acro mice propose the involvement of TCF20 in the upregulation of tumor's antioxidant genes, thereby promoting both tumor growth and metastasis (Figures 6A and 6B). We show that GHR and TCF20 inhibition attenuated GH-induced TNBC cell growth and invasion. NRF2 activation can stimulate lung metastasis by upregulating HO-1, leading to heme degradation, and reduced ROS levels.[28,29] Additionally, supplementing the diet of mice harboring tumors with a pharmacological or dietary (vitamin E) antioxidant promotes metastasis by

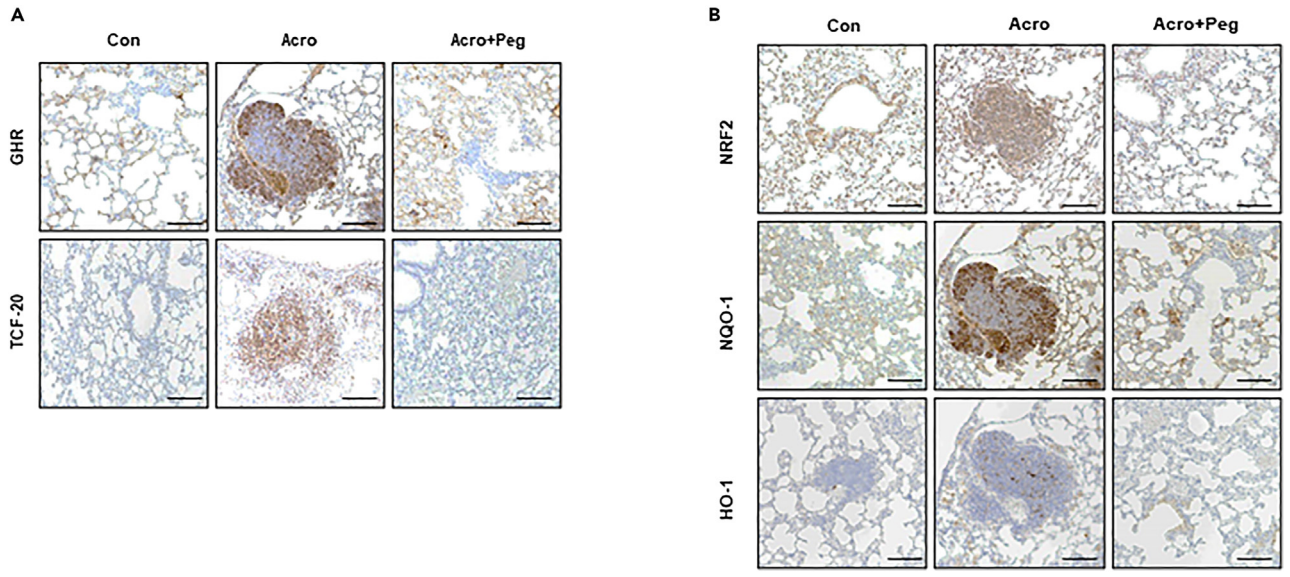

Figure 6. Excess endocrine GH induces TCF20 and antioxidant proteins in the metastatic lesion of acromegaly mice

(A and B) Representative images of lung tissue sections stained with (A) GHR, TCF20, (B) NRF2, NAD(P)H quinone dehydrogenase 1 (NQO-1), and heme oxygenase-1 (HO-1). Images were obtained at 200× magnification. Scale bar represents 100 μm.

increasing the intracellular Bach1.[27] We hypothesize that, similar to the other antioxidants, including N-acetylcysteine or vitamin E, excess endocrine GH may act as an antioxidant, contributing to tumor growth and metastasis by reducing ROS levels in breast cancer.

In conclusion, our results suggest that excess endocrine GH in acromegaly possesses a strong potential for promoting TNBC cell growth and metastasis. We identified a molecular mechanism involving the TCF20/NRF2 signaling axis activated by excess endocrine GH, which promotes TNBC progression. These insights may contribute to the development of strategies for the management of TNBC in patients with acromegaly.

Limitations of the study

This study has a few limitations. Firstly, our investigation primarily focused on the effects of excess GH. It's important to note that GH induces the production of IGF-1 in the liver, and excessive IGF-1 levels can also promote tumor growth and metastasis. However, we subcutaneously injected the GH antagonist around the peritumoral area and observed a reduction in tumor volume. Furthermore, we confirmed that there were no changes in the levels of TCF20/NRF2 in response to IGF-1. Additionally, comparable GH and IGF-1 levels were observed between Con mice and Acro mice in the mammary fat pad injected with Py230 cells. This underscores that the regulation of tumor growth and metastasis in acromegaly is orchestrated through the TCF20/NRF2 axis, induced by the excess endocrine GH. Secondly, we did not examine the effects of clinical data due to the rarity of acromegaly, making it challenging to obtain breast cancer tissue from affected patients at our institution.

STAR★METHODS

Detailed methods are provided in the online version of this paper and include the following:

- KEY RESOURCES TABLE
- RESOURCE AVAILABILITY
  - Lead contact
  - Materials availability
  - Data and code availability
- EXPERIMENTAL MODEL AND STUDY PARTICIPANT DETAILS
  - Animals and treatments
- METHOD DETAILS
  - Orthotopic injection of breast cancer cells
  - Tumor volume measurement
  - CMV-firefly-2A-GFP-Puro transduction in Py230
  - *In vivo* bioluminescence imaging
  - Transwell Matrigel invasion assay

- Wound healing assay
- RT^2 profiler polymerase chain reaction (PCR) arrays
- Cell cultures and reagents
- Small interfering ribonucleic acid (RNA) transfection
- RNA isolation and quantitative real-time PCR
- Western blot
- Enzyme-linked immunosorbent assay
- Immunohistochemistry

- QUANTIFICATION AND STATISTICAL ANALYSIS

SUPPLEMENTAL INFORMATION

Supplemental information can be found online at https://doi.org/10.1016/j.isci.2024.110137.

ACKNOWLEDGMENTS

We thank Flow Cytometry Core Facility in Yonsei University College of Medicine for their technical assistance. We appreciate the Medical Illustration & Design (MID) team, a member of Medical Research Support Services of Yonsei University College of Medicine, for their excellent support with the medical illustrations. Pegvisomant was kindly supported from Pfizer.

Funding: This research was supported by a grant from the Korea Health Technology R&D Project through the Korea Health Industry Development Institute (KHIDI), funded by the Ministry of Health & Welfare of the Republic of Korea [grant number: HR18C001208], and by the Basic Science Research Program through the National Research Foundation of Korea (NRF), funded by the Ministry of Education (NRF-2021R1I1A1A01052340).

AUTHOR CONTRIBUTIONS

Chan Woo Kang and Ju Hun Oh: Conceptualization, methodology, data curation, and writing-original draft preparation. Eun Kyung Wang, Yaru Bao, Ye Bin Kim, and Yang Jong Lee: Visualization and investigation. Eun Jig Lee, Cheol Ryong Ku, and Young Seok Jo: Supervision. Chan Woo Kang and Ju Hun Oh: Writing-reviewing and editing.

DECLARATION OF INTERESTS

The authors declare no conflict of interest.

Received: April 26, 2023
Revised: January 24, 2024
Accepted: May 27, 2024
Published: June 9, 2024

REFERENCES

1. Raben, M.S. (1962). Growth hormone. 1. Physiologic aspects. N. Engl. J. Med. *266*, 31–35. https://doi.org/10.1056/nejm196201042660109.
2. Greenwood, F.C., and Landon, J. (1966). Growth Hormone Secretion in Response to Stress in Man. Nature *210*, 540–541. https://doi.org/10.1038/210540a0.
3. Martin, J.B. (1973). Neural Regulation of Growth Hormone Secretion. N. Engl. J. Med. *288*, 1384–1393. https://doi.org/10.1056/nejm197306282882606.
4. Katznelson, L., Laws, E.R., Jr., Melmed, S., Molitch, M.E., Murad, M.H., Utz, A., and Wass, J.A.H.; Endocrine Society (2014). Acromegaly: An Endocrine Society Clinical Practice Guideline. J. Clin. Endocrinol. Metab. *99*, 3933–3951. https://doi.org/10.1210/jc.2014-2700.
5. Melmed, S., Colao, A., Barkan, A., Molitch, M., Grossman, A.B., Kleinberg, D., Clemmons, D., Chanson, P., Laws, E., Schlechte, J., et al. (2009). Guidelines for Acromegaly Management: An Update. J. Clin. Endocrinol. Metab. *94*, 1509–1517. https://doi.org/10.1210/jc.2008-2421.
6. Colao, A., Grasso, L.F.S., Giustina, A., Melmed, S., Chanson, P., Pereira, A.M., and Pivonello, R. (2019). Acromegaly. Nat. Rev. Dis. Primers *5*, 20. https://doi.org/10.1038/s41572-019-0071-6.
7. Zhang, W., Qian, P., Zhang, X., Zhang, M., Wang, H., Wu, M., Kong, X., Tan, S., Ding, K., Perry, J.K., et al. (2015). Autocrine/Paracrine Human Growth Hormone-stimulated MicroRNA 96-182-183 Cluster Promotes Epithelial-Mesenchymal Transition and Invasion in Breast Cancer. J. Biol. Chem. *290*, 13812–13829. https://doi.org/10.1074/jbc.M115.653261.
8. Waters, M.J., and Conway-Campbell, B.L. (2004). The oncogenic potential of autocrine human growth hormone in breast cancer. Proc. Natl. Acad. Sci. USA *101*, 14992–14993. https://doi.org/10.1073/pnas.0406396101.
9. Mukhina, S., Mertani, H.C., Guo, K., Lee, K.O., Gluckman, P.D., and Lobie, P.E. (2004). Phenotypic conversion of human mammary carcinoma cells by autocrine human growth hormone. Proc. Natl. Acad. Sci. USA *101*, 15166–15171. https://doi.org/10.1073/pnas.0405881101.
10. Subramani, R., Nandy, S.B., Pedroza, D.A., and Lakshmanaswamy, R. (2017). Role of Growth Hormone in Breast Cancer. Endocrinology *158*, 1543–1555. https://doi.org/10.1210/en.2016-1928.
11. Boguszewski, C.L., and Boguszewski, M.C.d.S. (2019). Growth Hormone's Links to Cancer. Endocr. Rev. *40*, 558–574. https://doi.org/10.1210/er.2018-00166.
12. Gillam, M.P., Ku, C.R., Lee, Y.J., Kim, J., Kim, S.H., Lee, S.J., Hwang, B., Koo, J., Kineman, R.D., Kiyokawa, H., and Lee, E.J. (2017). Somatotroph-Specific Aip-Deficient Mice Display Pretumorigenic Alterations in Cell-Cycle Signaling. J. Endocr. Soc. *1*, 78–95. https://doi.org/10.1210/js.2016-1004.
13. Boguszewski, C.L., and Ayuk, J. (2016). MANAGEMENT OF ENDOCRINE DISEASE: Acromegaly and cancer: an old debate revisited. Eur. J. Endocrinol. *175*, R147–R156. https://doi.org/10.1530/eje-16-0178.
14. Guevara-Aguirre, J., Balasubramanian, P., Guevara-Aguirre, M., Wei, M., Madia, F., Cheng, C.-W., Hwang, D., Martin-Montalvo, A., Saavedra, J., Ingles, S., et al. (2011). Growth Hormone Receptor Deficiency Is

Associated with a Major Reduction in Pro-Aging Signaling, Cancer, and Diabetes in Humans. Sci. Transl. Med. *3*, 70ra13. https://doi.org/10.1126/scitranslmed.3001845.

15. Arumugam, A., Subramani, R., Nandy, S.B., Terreros, D., Dwivedi, A.K., Saltzstein, E., and Lakshmanaswamy, R. (2019). Silencing growth hormone receptor inhibits estrogen receptor negative breast cancer through ATP-binding cassette sub-family G member 2. Exp. Mol. Med. *51*, 1–13. https://doi.org/10.1038/s12276-018-0197-8.
16. Perry, J.K., Wu, Z.-S., Mertani, H.C., Zhu, T., and Lobie, P.E. (2017). Tumour-Derived Human Growth Hormone As a Therapeutic Target in Oncology. Trends Endocrinol. Metab. *28*, 587–596. https://doi.org/10.1016/j.tem.2017.05.003.
17. Zhang, B., Shu, X.-O., Delahanty, R.J., Zeng, C., Michailidou, K., Bolla, M.K., Wang, Q., Dennis, J., Wen, W., Long, J., et al. (2015). Height and Breast Cancer Risk: Evidence From Prospective Studies and Mendelian Randomization. J. Natl. Cancer Inst. *107*, djv219. https://doi.org/10.1093/jnci/djv219.
18. Raccurt, M., Lobie, P.E., Moudilou, E., Garcia-Caballero, T., Frappart, L., Morel, G., and Mertani, H.C. (2002). High stromal and epithelial human gh gene expression is associated with proliferative disorders of the mammary gland. J. Endocrinol. *175*, 307–318. https://doi.org/10.1677/joe.0.1750307.
19. Kaulsay, K.K., Mertani, H.C., Törnell, J., Morel, G., Lee, K.-O., and Lobie, P.E. (1999). Autocrine Stimulation of Human Mammary Carcinoma Cell Proliferation by Human Growth Hormone. Exp. Cell Res. *250*, 35–50. https://doi.org/10.1006/excr.1999.4492.
20. Brittain, A.L., Basu, R., Qian, Y., and Kopchick, J.J. (2017). Growth Hormone and the Epithelial-to-Mesenchymal Transition. J. Clin. Endocrinol. Metab. *102*, 3662–3673. https://doi.org/10.1210/jc.2017-01000.
21. Shafiei, F., Rahnama, F., Pawella, L., Mitchell, M.D., Gluckman, P.D., and Lobie, P.E. (2008). DNMT3A and DNMT3B mediate autocrine hGH repression of plakoglobin gene transcription and consequent phenotypic conversion of mammary carcinoma cells. Oncogene *27*, 2602–2612. https://doi.org/10.1038/sj.onc.1210917.
22. Proestling, K., Birner, P., Gamperl, S., Nirtl, N., Marton, E., Yerlikaya, G., Wenzl, R., Streubel, B., and Husslein, H. (2015). Enhanced epithelial to mesenchymal transition (EMT) and upregulated MYC in ectopic lesions contribute independently to endometriosis. Reprod. Biol. Endocrinol. *13*, 75. https://doi.org/10.1186/s12958-015-0063-7.
23. Pandey, V., Perry, J.K., Mohankumar, K.M., Kong, X.J., Liu, S.M., Wu, Z.S., Mitchell, M.D., Zhu, T., and Lobie, P.E. (2008). Autocrine human growth hormone stimulates oncogenicity of endometrial carcinoma cells. Endocrinology *149*, 3909–3919. https://doi.org/10.1210/en.2008-0286.
24. Gugnoni, M., Sancisi, V., Gandolfi, G., Manzotti, G., Ragazzi, M., Giordano, D., Tamagnini, I., Tigano, M., Frasoldati, A., Piana, S., and Ciarrocchi, A. (2017). Cadherin-6 promotes EMT and cancer metastasis by restraining autophagy. Oncogene *36*, 667–677. https://doi.org/10.1038/onc.2016.237.
25. Subramani, R., Lopez-Valdez, R., Salcido, A., Boopalan, T., Arumugam, A., Nandy, S., and Lakshmanaswamy, R. (2014). Growth hormone receptor inhibition decreases the growth and metastasis of pancreatic ductal adenocarcinoma. Exp. Mol. Med. *46*, e117. https://doi.org/10.1038/emm.2014.61.
26. Darvekar, S.R., Elvenes, J., Brenne, H.B., Johansen, T., and Sjøttem, E. (2014). SPBP is a sulforaphane induced transcriptional coactivator of NRF2 regulating expression of the autophagy receptor p62/SQSTM1. PLoS One *9*, e85262. https://doi.org/10.1371/journal.pone.0085262.
27. Wiel, C., Le Gal, K., Ibrahim, M.X., Jahangir, C.A., Kashif, M., Yao, H., Ziegler, D.V., Xu, X., Ghosh, T., Mondal, T., et al. (2019). BACH1 Stabilization by Antioxidants Stimulates Lung Cancer Metastasis. Cell *178*, 330–345.e22. https://doi.org/10.1016/j.cell.2019.06.005.
28. Wang, H., Liu, X., Long, M., Huang, Y., Zhang, L., Zhang, R., Zheng, Y., Liao, X., Wang, Y., Liao, Q., et al. (2016). NRF2 activation by antioxidant antidiabetic agents accelerates tumor metastasis. Sci. Transl. Med. *8*, 334ra51. https://doi.org/10.1126/scitranslmed.aad6095.
29. Lignitto, L., LeBoeuf, S.E., Homer, H., Jiang, S., Askenazi, M., Karakousi, T.R., Pass, H.I., Bhutkar, A.J., Tsirigos, A., Ueberheide, B., et al. (2019). Nrf2 Activation Promotes Lung Cancer Metastasis by Inhibiting the Degradation of Bach1. Cell *178*, 316–329.e18. https://doi.org/10.1016/j.cell.2019.06.003.
30. Chesnokova, V., Zonis, S., Zhou, C., Recouvreux, M.V., Ben-Shlomo, A., Araki, T., Barrett, R., Workman, M., Wawrowsky, K., Ljubimov, V.A., et al. (2016). Growth hormone is permissive for neoplastic colon growth. Proc. Natl. Acad. Sci. USA *113*, E3250–E3259. https://doi.org/10.1073/pnas.1600561113.
31. Basu, R., and Kopchick, J.J. (2019). The effects of growth hormone on therapy resistance in cancer. Cancer Drug Resist. *2*, 827–846. https://doi.org/10.20517/cdr.2019.27.
32. Chesnokova, V., and Melmed, S. (2019). Growth hormone in the tumor microenvironment. Arch. Endocrinol. Metab. *63*, 568–575. https://doi.org/10.20945/2359-3997000000186.
33. Basu, R., Qian, Y., Mathes, S., Terry, J., Arnett, N., Riddell, T., Stevens, A., Funk, K., Bell, S., Bokal, Z., et al. (2022). Growth hormone receptor antagonism downregulates ATP-binding cassette transporters contributing to improved drug efficacy against melanoma and hepatocarcinoma in vivo. Front. Oncol. *12*, 936145. https://doi.org/10.3389/fonc.2022.936145.
34. Evans, A., Jamieson, S.M.F., Liu, D.-X., Wilson, W.R., and Perry, J.K. (2016). Growth hormone receptor antagonism suppresses tumour regrowth after radiotherapy in an endometrial cancer xenograft model. Cancer Lett. *379*, 117–123. https://doi.org/10.1016/j.canlet.2016.05.031.
35. Hedrington, M.S., and Davis, S.N. (2015). Sexual Dimorphism in Glucose and Lipid Metabolism during Fasting, Hypoglycemia, and Exercise. Front. Endocrinol. *6*, 61. https://doi.org/10.3389/fendo.2015.00061.
36. Leung, K.C., Johannsson, G., Leong, G.M., and Ho, K.K.Y. (2004). Estrogen regulation of growth hormone action. Endocr. Rev. *25*, 693–721. https://doi.org/10.1210/er.2003-0035.
37. Sayin, V.I., Ibrahim, M.X., Larsson, E., Nilsson, J.A., Lindahl, P., and Bergo, M.O. (2014). Antioxidants Accelerate Lung Cancer Progression in Mice. Sci. Transl. Med. *6*, 221ra15. https://doi.org/10.1126/scitranslmed.3007653.
38. Gong, Y., Zhang, K., Xiong, D., Wei, J., Tan, H., and Qin, S. (2020). Growth hormone alleviates oxidative stress and improves the IVF outcomes of poor ovarian responders: a randomized controlled trial. Reprod. Biol. Endocrinol. *18*, 91. https://doi.org/10.1186/s12958-020-00648-2.
39. Luque, R.M., Amargo, G., Ishii, S., Lobe, C., Franks, R., Kiyokawa, H., and Kineman, R.D. (2007). Reporter Expression, Induced by a Growth Hormone Promoter-Driven Cre Recombinase (rGHp-Cre) Transgene, Questions the Developmental Relationship between Somatotropes and Lactotropes in the Adult Mouse Pituitary Gland. Endocrinology *148*, 1946–1953. https://doi.org/10.1210/en.2006-1542.
40. Tavera-Mendoza, L.E., and Brown, M. (2017). A less invasive method for orthotopic injection of breast cancer cells into the mouse mammary gland. Lab. Anim. *51*, 85–88. https://doi.org/10.1177/0023677216640706.
41. Kocatürk, B., and Versteeg, H.H. (2015). Orthotopic injection of breast cancer cells into the mammary fat pad of mice to study tumor growth. J. Vis. Exp. *96*, 51967. https://doi.org/10.3791/51967.
42. Lee, M.W., Kim, H.J., Yoo, K.H., Kim, D.S., Yang, J.M., Kim, H.R., Noh, Y.H., Baek, H., Kwon, H., Son, M.H., et al. (2012). Establishment of a bioluminescent imaging-based in vivo leukemia model by intra-bone marrow injection. Int. J. Oncol. *41*, 2047–2056. https://doi.org/10.3892/ijo.2012.1634.
43. Peng, Y., Zhang, H.W., Cao, W.H., Mao, Y., and Cheng, R.C. (2020). Exploration of the Potential Biomarkers of Papillary Thyroid Cancer (PTC) Based on RT(2) Profiler PCR Arrays and Bioinformatics Analysis. Cancer Manag. Res. *12*, 9235–9246. https://doi.org/10.2147/cmar.S266473.

STAR★METHODS

KEY RESOURCES TABLE

REAGENT or RESOURCE	SOURCE	IDENTIFIER
Antibodies		
TCF20	Novus Biologicals	Cat#NBP2-83631; RRID:AB_2922977
GHR	Santa Cruz	Cat#sc-137185; RRID:AB_2111405
NQO-1	Santa Cruz	Cat#sc-376023; RRID:AB_10987895
HO-1	Cell Signaling Technology	Cat#43966; RRID:AB_2799254
p-STAT5	Cell Signaling Technology	Cat#4322; RRID:AB_10544692
STAT5	Cell Signaling Technology	Cat#94205; RRID:AB_2737403
NRF2	Santa Cruz	Cat#sc-365949; RRID:AB_10917561
Lamin B1	PROTEINTECH	Cat#12987-1-AP; RRID:AB_2136290
GAPDH	Santa Cruz	Cat#sc-365062; RRID:AB_10847862
β-actin	Santa Cruz	Cat#sc-47778; RRID:AB_626632
Bacterial and virus strains		
Lentivirus (CMV-firefly-2A-GFP puro)	GenTarget	Cat#LVP020
Chemicals, peptides, and recombinant proteins		
RNAlater Solution	Thermo Fisher	Cat#AM7021
Fetal bovine serum (FBS)	Hyclone	Cat#SV30207.02
Penicillin/streptomycin	Hyclone	Cat#SV30010
Lipofectamine RNAiMAX reagent	Thermo Fisher	Cat#13778075
Cell lysis buffer	Cell signaling technology	Cat#9803
Protease inhibitor	Sigma-Aldrich	Cat#P8340
Phosphatase inhibitor 2	Sigma-Aldrich	Cat#P5726
Phosphatase inhibitor 3	Sigma-Aldrich	Cat#P0044
PMSF	Sigma-Aldrich	Cat#P7626
WESTSAVEup	Ab Frontier	Cat#LF-QC 0101
Power SYBR Green PCR Master Mix	Applied Biosystems	Cat#4367659
MTS reagent	Promega	Cat#G3580
Mito+serum extender	Corning	Cat#355006
Recombinant human growth hormone	Biovision	Cat#4769
Recombinant human IGF-1	R&D systems	Cat#291-G1
Opti-MEM	Thermo Fisher	Cat#31985070
TRIzol	Takara	Cat#9108
Pegvisomant	Pfizer	N/A
Matrigel	Corning	Cat#CLS356231
Critical commercial assays		
Bicinchoninic Acid (BCA) protein assay kit	Thermo Fisher	Cat#23227
ReverTra Ace qPCR RT Mix kit	TOYOBO	Cat#TOFSQ-101
NE-PER Nuclear and cytoplasmic extraction kit	Thermo Fisher	Cat#78833
Mouse growth hormone ELISA kit	Millipore	Cat#EZRMGH-45K
Mouse IGF1 ELISA kit	Abcam	Cat#Ab100695
Estradiol parameter assay kit	R&D sytems	Cat#KGE014
Matrigel invasion assay kit	Corning	Cat#DLW354480

(*Continued on next page*)

Continued

REAGENT or RESOURCE	SOURCE	IDENTIFIER
Real-time RT2 Profiler polymerase chain reaction array	Qiagen	Cat#PAMM-028Z
Experimental models: Cell lines		
Mouse: Py230	American Type Culture Collection	CRL-3279
Human: MDA-MB-231	American Type Culture Collection	HTB-26
Human: Hs578T	American Type Culture Collection	HTB-126
Human: HCC1806	Korean Cell Line Bank	9S1806
Experimental models: Organisms/strains		
Mouse: rGHp-Cre$^{tg/+}$; Aip$^{lox/lox}$	Gillam et al.	Gillam et al.[12]
Mouse: Aip$^{lox/lox}$	Gillam et al.	Gillam et al.[12]
Oligonucleotides		
Real-time PCR primers, see Table S1	This paper	N/A
siRNA for transfection, see Table S2	Thermo Fisher Scientific, Bioneer	N/A
Software and algorithms		
ImageJ	NIH	RRID:SCR_003070
Prism software v.4.0.0	GraphPad Inc.	https://www.graphpad.com/
R package	R CRAN	http://www.R-project.org/
Other		
ViiA™ 7 Real-time PCR system	Applied Biosystems	N/A
Microscope	Nikon	Cat#DS-Ri2
IVIS	Perkin Elmer	Cat#CLS136334
iBright FL1500	Thermo Fisher	Cat# A44115

RESOURCE AVAILABILITY

Lead contact

Further information and requests for resources and reagents should be directed to and will be fulfilled by the lead contact, Eun Jig Lee (ejlee423@yuhs.ac).

Materials availability

This study did not generate new unique reagents. The rGHp-Cre$^{tg/+}$; Aip$^{lox/lox}$ and Aip$^{lox/lox}$ mouse in this study should be directed to and will be fulfilled by the lead contact Eun Jig Lee (ejlee423@yuhs.ac).

Data and code availability

- All data reported in this paper will be shared by the lead contact upon request.
- This paper does not report original or code.
- Any additional information required to reanalyze the data reported in this work paper is available from the lead contact upon request.

EXPERIMENTAL MODEL AND STUDY PARTICIPANT DETAILS

Animals and treatments

Animal model used in this study was a previously established mouse model in our laboratory, which expresses the phenotype of GH-secreting pituitary adenoma.[12] Somatotroph-specific aryl hydrocarbon receptor interacting protein (AIP) knockout (sAIPKO) mouse model was made using rGHp-Cre$^{tg/+}$; Aip$^{lox/lox}$ mice.[39] The Aip locus was targeted through homologous recombination in embryonic stem cells using the C57BL/6 strain.[12] Aip$^{lox/lox}$ mice were used as controls. All animals in this study were females over 24 weeks old because sAIPKO mice exhibited elevated endocrine GH as they aged compare to the Aip$^{lox/lox}$ mice. Mice were maintained under controlled conditions (12-h light: 12-h darkness cycle, 21°C) and were provided free access to laboratory chow and tap water. All procedures involving animal subjects were approved by the Institutional Animal Care and Use Committee (IACUC) at Yonsei University College of Medicine (IACUC: 2019-0141).

Pegvisomant was generously provided by Pfizer. We administered pegvisomant at a dose of 10 mg/kg via subcutaneous injection around the tumor site 4 weeks after the orthotopic injection.

METHOD DETAILS

Orthotopic injection of breast cancer cells

Orthotopic injection of breast cancer cells into the mammary fat pad was performed and modified according to the previous study.[40,41] On the day of operation, the Py230 cells derived from C57BL/6 mice were washed once with phosphate-buffered saline (PBS) and trypsinized. Trypsin was quenched by adding 10 mL of serum containing Dulbecco's Modified Eagle Medium (DMEM). The cells were centrifuged at 300×g for 5 min to remove the serum by resuspending the cells in serum-free media. The cells were centrifuged again to remove the remaining serum completely and resuspended in media. Subsequently, the cells were counted, and 500,000 cells/mouse were used in 150 μL. The cells were resuspended in Matrigel and kept on ice. Forty-week-old female mice were anesthetized using 3% inhalant isoflurane. The mice were fixed on a heating pad. The area around the fourth nipple was shaved and cleaned using an ethanol cotton swab. A small incision was made between the fourth nipple and the midline using a scissor, and a pocket was made by inserting the cotton swab moistened with PBS (pH 7.4). The mammary fat pad was squeezed using a tweezer to expose the fat pad to perform the injection easily. The cell mixture was homogenized by pipetting up and down. Py230 cells were then injected using an insulin syringe with a volume of $\leq$120 μL. Successful injection was confirmed by the swelling of the tissue. The incision site was sutured. All procedures involving animal subjects were approved by the IACUC at Yonsei University College of Medicine (IACUC: 2019-0141).

Tumor volume measurement

The length, width of the tumor mass was measured every 2 days using calipers, and tumor volume was calculated as follows: tumor volume = 0.5236 × length × width^2 (mm^3).

CMV-firefly-2A-GFP-Puro transduction in Py230

Pre-made lentivirus CMV-firefly-2A-GFP-Puro (Cat# LVP020; GenTarget Inc., San Diego, CA, USA) transduction was conducted according to the manufacturer's instructions. Briefly, the cells were seeded in complete medium at 50%–75% confluency and incubated overnight. The next day, the pre-made lentiviral stock was thawed at room temperature, and 50 μL of virus stock was added to obtain the desired multiplicity of infection. After 72 h without changing the medium, the positive transduction rate was visualized by fluorescence microscopy. Transduced cells were sorted by fluorescence-activated cell sorting and selected for antibiotic resistance.

In vivo bioluminescence imaging

After the breast cancer injection, bioluminescence imaging was performed every week. On the day of imaging, mice were intraperitoneally injected with D-luciferin (150 mg/kg) and were placed in a light-tight mouse imaging chamber following anesthesia. Twenty minutes after the injection, each animal was imaged alone in supine and prone positions with an exposure time of 10 min for each position weekly for 6 weeks using *in vivo* imaging system (IVIS) Spectrum (Xenogen, Alameda, CA, USA). Regions of interest (ROIs) were analyzed, and total quantification of bioluminescence was performed using the Living Image (Xenogen) software. Photons detected from breast cancer models were converted to average radiance (photon/sec/cm^2/sr). Average radiance values are quantitative data obtained from the ROIs where photons are emitted by bioluminescent cells of the assigned rectangular area over the whole body of each mouse. Both luminescence and image data were analyzed using the Living Image software.[42]

Transwell Matrigel invasion assay

Breast cancer cells were seeded to the Matrigel-coated transwell insert, and 0.75 mL of chemoattractant was added to the lower wells. Cell invasion chambers were incubated overnight in a humidified tissue culture incubator. After the incubation, non-invading cells were removed from the upper side of the Matrigel-coated side by scrubbing. The invaded cells to the lower surface of the Matrigel were stained with 0.1% crystal violet and rinsed with distilled water. The dried Matrigel was placed on a slide, added with a drop of immersion oil, and covered with a coverslip.

Wound healing assay

Py230 cells were seeded at 1 × 10^6 cells/well in a 6-well plate for 100% confluence in 24 h. In a sterile environment, a 200 μL pipette tip was used to press firmly against the top of the tissue culture plate, and a vertical wound was swiftly made down through the cell monolayer. The media and cell debris were carefully aspirated, and a sufficient volume of culture media was slowly added against the well wall to cover the well. A snapshot picture was taken, and the plate was assessed for wound closure.

RT^2 profiler polymerase chain reaction (PCR) arrays

The amplified copy deoxyribonucleic acid (cDNA) was used on the real-time RT^2 Profiler polymerase chain reaction (PCR) array (QIAGEN, Cat. no. PAMM-028Z) in combination with RT^2 SYBRGreen Real-time PCR Mastermix (Cat. no. 330529). Each array plate contained one set of 96 wells for testing. Genomic DNA contamination, reverse transcription, and positive PCR controls were included in each 96-well set on each plate. *β-actin* was used as the assay reference gene. Cycle threshold (CT) values were derived to an Excel file to build a table of CT values, which was then uploaded onto the data analysis web portal at http://www.qiagen.com/geneglobe. The samples contained both the control and test groups. CT values were normalized based on an automatic selection from the full panel of reference genes.[43]

Cell cultures and reagents

Mouse triple-negative breast cancer (TNBC) cell line Py230 was purchased from the American Type Culture Collection and cultured in DMEM replenished with 10% fetal bovine serum (FBS; Hyclone Co., Logan, UT, USA), 1% Pen/Strep (Hyclone Co., Logan, UT, USA), and 0.1% MITO+ Serum Extender (Corning #355006). Py230 cells do not maintain their properties without the MITO+ Serum Extender. Human breast cancer cell lines Hs578T and MDA-MB-231 were purchased from the American Type Culture Collection and cultured in DMEM replenished with 10% FBS (Hyclone Co., Logan, UT, USA) and 1% Pen/Strep (Hyclone Co., Logan, UT, USA). Human breast cancer cell line HCC1806 was purchased from Korean Cell Line Bank (Seoul, Korea) and cultured in Roswell Park Memorial Institute (RPMI) replenished with 10% FBS and 1% Pen/Strep. All cell lines were grown in a culture incubator that maintained the atmospheric condition of 37°C and 5% CO_2. The media were changed within 3 days, and the cells were split with trypsin/ethylenediamine tetraacetic acid every week.

Recombinant human GH (Bio Vision, Waltham, MA, USA) and recombinant human IGF-1(R&D systems, Minneapolis, MN, USA) were reconstituted in the culture medium containing 0.1% bovine serum albumin (BSA). Cells were placed in the culture medium free of serum containing 0.1% BSA, GH or IGF-1 were added, and cells were harvested 24 h later. If treatment was extended to 48 h, GH was added daily.[30] against phosphorylated signal transducer and activator of transcription 5 (STAT5), STAT5, heme oxygenase-1 (HO-1), and histone H3 were purchased from Cell Signaling Technology (Danvers, MA, USA). β-actin and GHR were purchased from Santa Cruz Biotechnology (Dallas, TX, USA).

Small interfering ribonucleic acid (RNA) transfection

Small interfering ribonucleic acids (siRNAs) targeting mouse *GHR* (UAU AAU UUC UGU UUA CUG C), mouse *TCF20* (UAU UUA UAU AUA UAU AUU C), human *GHR* (UAU AAU UUC UGU UUA CUG C), and human *TCF20* (UAU ACU GCA UCA CAU GCU GAG AAG G) were purchased from Thermo Fisher Scientific (Waltham, MA, USA). Py230 and Hs578T cells were seeded at 0.8×10^6 cells/well in the 6-well plate 24 h before transfection. siRNAs were transfected using Lipofectamine RNAiMAX reagent (Thermo Fisher Scientific) in Opti-MEM media (Thermo Fisher Scientific) for 16 h. Media were changed into the culture media on the next day and incubated for an additional 24 h before analysis.

RNA isolation and quantitative real-time PCR

Total RNA was isolated using NucleoZOL (Macherey-Nagel, Duren, Germany) followed by reverse transcription (ReverTra Ace-α; TOYOBO, Osaka, Japan) according to the manufacturers' instructions. The resulting cDNA was subjected to quantitative real-time PCR with Power SYBRGreen Master Mix (4367659; Thermo Fisher Scientific) using the StepOnePlusTM Real-Time PCR System (Applied Biosystems, Carlsbad, CA, USA) according to the manufacturers' instructions. The primers used in this study are listed in Table S1.

Western blot

Total protein samples were isolated from frozen primary breast cancer and metastatic tumor and cultured cells using cell lysis buffer (Cell Signaling Technology, Beverly, MA, USA) containing protease and phosphatase inhibitors (Roche, Basel, Switzerland). Samples were lysed on ice for 30 min and then centrifuged for 15 min at 13,000 rpm at 4°C. Proteins were separated in a 10% sodium dodecyl sulfate-polyacrylamide gel electrophoresis and transferred onto activated polyvinylidene difluoride membranes. Membranes were blocked in 5% skim milk and incubated with specific primary antibodies at 1:1000 in Tris-Buffered Saline with Tween. After primary and secondary antibody incubations, the blots were visualized using WESTSAVEup (west blotting substrate) and exposed to X-ray film (Agfa HealthCare). Nucleus and cytosol proteins were separated using the NE-PER Nuclear and Cytoplasmic Extraction kit (Thermo Fisher Scientific) according to the manufacturer's instructions.

Enzyme-linked immunosorbent assay

Blood samples were collected after the mice were sacrificed following an overnight fast, and serum and plasma samples were stored at −80°C. Mouse GH enzyme-linked immunosorbent assay (ELISA) kit 96-well plate (Millipore, Billerica, MA, USA), mouse IGF-1 ELISA kit (Abcam, Cambridge, UK), and mouse estradiol ELISA kit (R&D systems, MN. USA) were used according to the manufacturers' instructions.

Immunohistochemistry

Mouse primary and lung metastatic tumors were fixed in 10% formalin. Tissue sections of 5 μm thickness were cut from each block to perform either hematoxylin and eosin (H&E) or immunostaining with TCF20, NRF2, HO-1, Nqo-1, and GHR antibodies. After dewaxing and rehydrating paraffin sections and antigen retrieval by transcriptional regulatory sequence low or high buffer for each antibody condition, tissue sections were immunolabeled with the following primary antibodies: rabbit anti-TCF20 (1:200, Novus Biologicals, CO, USA), mouse anti-GHR (1:250, Santa Cruz, CA, USA), mouse anti-NQO-1 (1:250, Santa Cruz, CA, USA), and rabbit anti-HO-1 (1:250, Cell Signaling Technology). All slides were counterstained with hematoxylin.

QUANTIFICATION AND STATISTICAL ANALYSIS

Data were analyzed by GraphPad Prism Software. Differences between the two groups were compared using unpaired Student's t-tests. All data were expressed as means ± SEM. Statistical significance was accepted when $p < 0.05$. All details were shown in figure legends.